

Coreless vortex dipoles and bubbles in phase-separated binary condensates

S. Gautam,¹ P. Muruganandam,² and D. Angom¹

¹Physical Research Laboratory, Navarangpura, Ahmedabad - 380 009, India

²School of Physics, Bharathidasan University, Tiruchirapalli 620 024, Tamil Nadu, India

(Dated: May 31, 2022)

Vortex dipoles are generated when an obstacle moves through a superfluid. In case of phase-separated binary condensates, with appropriate interaction parameters in pan-cake shaped traps, we show that coreless vortex dipoles are created when a Gaussian obstacle beam traverses across them above a critical speed. As the obstacle passes through the inner component, it carries along a bubble of the outer component. Using Thomas-Fermi approximation, we show that phase-separated binary condensates can either support vortices with empty or filled cores. For time dependent obstacle potentials, ramped down in the present case, relative energy scales of the system influence the dynamical evolution of the binary condensate.

PACS numbers: 03.75.Lm,03.75.Kk,03.75.Mn

Vortices are among the most fundamental topological structures in fluid flows. These occur in a variety of fluids at different length scales and in different settings. In Bose-Einstein condensates (BECs), vortices carry integral angular momenta and serve as evidence of superfluidity. Formation and dynamics of solitary and multiple vortices in single species condensates is well studied. These vortices with empty cores and a phase singularity at the center of the cores are *normal vortices*, whose analogues are found in variety of other fluids. An important development in vortex dynamics is the realization of vortex dipoles, a pair of vortex and anti-vortex, due to superfluid flow past an obstacle [1]. Furthermore, the recent development to observe vortex dipoles in real time [2] opens up the possibility to examine dynamics. The vortex dipoles can also be considered as the embedded section of a vortex ring, which were first observed in BEC as decay product of dark solitons [3]. Another phenomenon in superfluids, where vortex dipoles are crucial is transition to quantum turbulence. The initial requirement is the formation of multiple vortex dipoles, followed by reconnections to form a vortex tangle, which then leads to quantum turbulence [4]. In multi-component condensates, coreless vortices [5] and Skyrmions [6] have been experimentally observed in spinor condensates. Coreless vortices in multi-component spinless condensates are, however, yet to be experimentally realized.

Theoretically, the flow of the miscible binary and spinor condensates across a Gaussian obstacle potential has been investigated [7–9]. A related work is the seeding of vortex rings when a condensate bubble moves through the bulk of another condensate in binary condensates. This is examined in a recent work [10]. In addition, phase-separated binary condensates, under suitable conditions, are appropriate systems to observe phenomena related to dynamical instabilities. These include, modulational instability [11, 12], Kelvin-Helmholtz instability [13], Rayleigh-Taylor instability [14, 15], countersuperflow instability [16, 17] and Richtmyer-Meshkov instabil-

ity [18]. Among these, the countersuperflow instability was recently realized experimentally [19]. Phase separation, which has been observed experimentally [20, 21], is also a necessary condition to observe coreless vortex dipoles with a moving obstacle.

In this letter we report the theoretical study of vortex dipole formation when a Gaussian obstacle moves through phase-separated binary condensates. As a specific case, we consider the binary condensate consisting of ⁸⁵Rb and ⁸⁷Rb. In this, one of the scattering lengths can be tuned by using magnetic Feshbach resonances [20]. This allows us to choose values of scattering lengths suitable for generation of coreless vortex dipoles.

BINARY CONDENSATES AND VORTEX DIPOLES

Dynamics of weakly interacting binary condensate at zero temperature is well described by a set of coupled GP equations

$$\left[\frac{-\hbar^2}{2m} \nabla^2 + V_i(\mathbf{r}, t) + \sum_{j=1}^2 U_{ij} |\Psi_j(\mathbf{r}, t)|^2 - i\hbar \frac{\partial}{\partial t} \right] \Psi_i(\mathbf{r}, t) = 0 \quad (1)$$

in mean field approximation, where $i = 1, 2$ is the species index. Here $U_{ii} = 4\pi\hbar^2 a_{ii}/m_i$, where m_i is the mass and a_{ii} is the s -wave scattering length, is the intra-species interaction, $U_{ij} = 2\pi\hbar^2 a_{ij}/m_{ij}$, where $m_{ij} = m_i m_j / (m_i + m_j)$ is the reduced mass and a_{ij} is the inter-species scattering length, is the inter-species interaction, and $V_i(\mathbf{r})$ is the trapping potential experienced by i th species. In the present work, we consider binary condensate consisting of ⁸⁵Rb and ⁸⁷Rb for which $m_1 \approx m_2$.

Furthermore, we also consider identical trapping potentials, which are axially symmetric, for both the species. The total potential is then

$$V(\mathbf{r}, t) = \frac{m\omega^2}{2} (x^2 + y^2 + \beta^2 z^2) + V_{\text{obs}}(x, y, t),$$

where $V_{\text{obs}}(x, y, t) = V_0(t) \exp\{-2([x - x_0(t)]^2 + y^2)/w_0^2\}$ is the blue detuned Gaussian obstacle potential and β is the anisotropy parameter. Define the oscillator length of the trapping potential $a_{\text{osc}} = \sqrt{\hbar/(m\omega)}$, and consider $\hbar\omega$ as the unit of energy. We can then rewrite the equations in dimensionless form with transformations $\tilde{\mathbf{r}} = \mathbf{r}/a_{\text{osc}}$, $\tilde{t} = t\omega$ and $\phi_i(\tilde{\mathbf{r}}, \tilde{t}) = \sqrt{a_{\text{osc}}^3/N_i} \Psi_i(\mathbf{r}, t)$. In pancake-shaped traps ($\beta \gg 1$), $\phi(\mathbf{r}, t) = \psi(x, y, t)\zeta(z) \exp(-i\beta t/2)$ [22], where $\zeta = (\beta/(2\pi))^{1/4} \exp(-\beta z^2/4)$ is the ground state wave function in axial direction. The Eq. (1) can then be reduced to the two dimensional form

$$\left[-\frac{1}{2} \left(\frac{\partial^2}{\partial x^2} + \frac{\partial^2}{\partial y^2} \right) + \frac{x^2 + \alpha_i^2 y^2}{2} + V_{\text{obs}}(x, y, t) + \sum_{j=1}^2 u_{ij} |\psi_j(\mathbf{r}, t)|^2 - i \frac{\partial}{\partial t} \right] \psi_i(\mathbf{r}, t) = 0, \quad (2)$$

where $u_{ii} = 2a_{ii}N_i\sqrt{2\pi\beta_i}/a_{\text{osc}}$ and $u_{ij} = 2a_{ij}N_j\sqrt{2\pi\beta_i}/a_{\text{osc}}$. Here we have neglected a constant term corresponding to energy along axial direction as it only shifts the energies and chemical potentials by a constant number without affecting the dynamics. In the present work, we consider $u_{12} > \sqrt{u_{11}u_{22}}$ so that the ground state of the binary condensate is phase-separated. Geometry of the density distribution is such that the species with the lower repulsion energy forms a core and the other species forms a shell around it. For convenience, we identify the former and later as the first and second species, respectively. With this labelling, interaction energies $u_{11} < u_{22}$ and for equal populations, this implies $a_{11} < a_{22}$.

To be specific, we consider ^{85}Rb - ^{87}Rb binary condensate with $a_{11} = 460a_0$, $a_{22} = 99a_0$, and $a_{12} = 214a_0$ as the scattering length values and $2N_1 = N_2 = 10^6$ as the number of atoms. Here a_{11} is tunable with magnetic Feshbach resonance [23]. With these set of parameters, the stationary state of ^{85}Rb - ^{87}Rb binary condensate is just phase-separated. The trapping potential and obstacle laser potential parameters are same as those considered in Ref. [1], i.e. $\omega/(2\pi) = 8\text{Hz}$, $\alpha = 1$, $\beta = 11.25$, $V_0(0) = 93.0\hbar\omega$, and $w_0 = 10\mu\text{m}$. Hereafter we term this set of scattering lengths, number of atoms and trapping potential parameters as *set a*.

In hydrodynamics, the velocity field of a vortex dipole is the vector sum of two component fields. One of the fields arises due to the inhomogeneous density of the condensate and leads to the precession of an off center vortex around the trap center [24, 25]. In addition to this, each vortex has a velocity field which varies inversely with the distance from its center, which is experienced by the other vortex of vortex dipole. In the present work, we move the obstacle along x -axis and generate vortex dipoles located symmetrically about x -axis. If (x, y) and $(x, -y)$ are the locations of the positively and negatively charged vortices of the vortex dipole, respectively, then

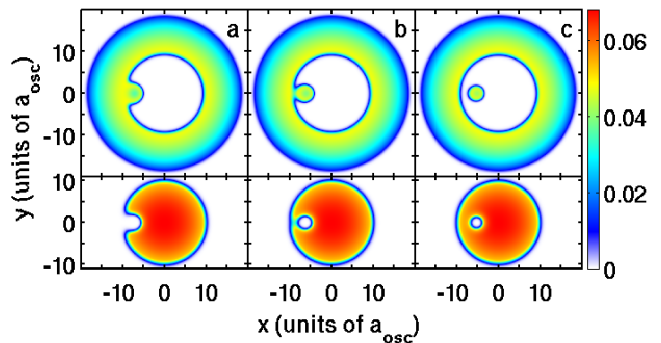


FIG. 1. (Color online) Stationary state $|\psi|$ of binary condensate with obstacle potential at (a) $-6.0a_{\text{osc}}$, (b) $-5.9a_{\text{osc}}$ and (c) $-5.0a_{\text{osc}}$.

the velocity field of the positively charged vortex is

$$\mathbf{v}(x, y) = \omega_{\text{pr}} \hat{k} \times \mathbf{r} + \frac{1}{2y} \hat{i},$$

where ω_{pr} is the rotational frequency of a vortex with charge $+1$ in the condensate. A similar equation describes the velocity field of the negatively charged vortex.

OBSTACLE MODIFIED DENSITY

To examine the density perturbations from the obstacle beam, let R_{in} be the radius of the inner species or the interface boundary. And, let R_{out} be the radial extent of the outer species. In the absence of the obstacle beam, the chemical potential of first and second species in scaled units are $\mu_1 = R_{\text{in}}^2/4 + u_{11}/(\pi R_{\text{in}}^2)$ and $R_{\text{out}}^2/2$, respectively. The obstacle beam initially ($t = 0$) located at $(-R_{\text{out}}, 0)$ traverses towards the center with velocity v_{obs} and the intensity is ramped down at the rate $-\partial V_0/\partial t = \eta$. The location of the beam at a later time is $x_0(t) = -R_{\text{out}} + v_{\text{ob}}t$, and intensity of the beam is $V_0(t) = V_0(0) - \eta t$, where $V_0(0)$ is the initial intensity of the obstacle beam. At the starting point, the total potential $V(R_{\text{out}}, 0, 0) > R_{\text{out}}^2/2$ and the density of the outer species $|\psi_2|^2$ is zero around the center of the obstacle beam. However, as it traverses the condensates with decreasing intensity, at some later time t' , $V(x_0(t'), 0, 0) < R_{\text{out}}^2/2$. Density $|\psi_2|^2$ is then finite within the obstacle. For compact notations, hereafter we drop the explicit notation of time dependence while writing $x_0(t)$ and $V_0(t)$.

A critical requirement to form coreless vortices is complete immersion of the obstacle beam within n_1 . Based on the previous discussions, as the beam approaches the origin, the last point of contact between the beam and interface at R_{in} lies along x -axis. To determine the condition when complete immersion occurs, consider the total

potential along x -axis around the obstacle potential

$$V(x, 0, t) \approx \frac{x^2}{2} + V_0(t) \left[1 - 2 \frac{(x - x_0(t))^2}{w^2} + 4 \frac{(x - x_0(t))^4}{w^4} \right], \quad (3)$$

where, the Gaussian beam potential is considered up to the second order term. The expression is appropriate in the neighborhood of the beam, and along x -axis it has one local minima (x_{\min}) and maxima each. There is also a global minima, however, it is not the correct solution as it lies in the domain where $x > w/\sqrt{2}$ and hence outside the domain of validity of Eq. (3). Correct global minima is located at $x \approx 0$ and is associated with the harmonic potential. The obstacle is considered well immersed when x_{\min} is located at the interfacial radius R_{in} , and let t_{im} be the time when it occurs.

When the obstacle beam is well inside the inner species, within the obstacle beam n_1 is zero but n_2 is nonzero. It then forms a second interface layer, which embeds a bubble of the n_2 within n_1 . Recollect, the first interface layer is located at R_{in} and it is where n_2 encloses n_1 . The second interface, unlike the one at R_{in} , is a deformed-ellipse and we label it as Γ . Around the interface, the two condensates mix with a penetration depth

$$\Lambda_i = \xi_i \left[\frac{\sqrt{a_{11}a_{22}}}{a_{12} - \sqrt{a_{11}a_{22}}} \right]^{1/2},$$

and the density of the minority species decays exponentially.

The transition from a single continuous interface to two separate boundaries at R_{in} and Γ , when the obstacle crosses R_{in} , is smooth in TF approximation and that is how we have defined t_{im} . There are, however, strong perturbations when surface tension is considered, and the separation of the two interfaces occurs when the beam is deep inside n_1 . Prior to the separation, the interface is deformed to accommodate a long neck region where n_1 and n_2 are non zero. As the interface splits into two, there are large deformations from the equilibrium interface geometry, and surface tension generates a restoring force to bring it to equilibrium geometry. This creates density patterns with high curvature and initiates formation of the coreless vortex dipoles.

OBSTACLE ASSISTED BUBBLE

At a time Δt after the obstacle is immersed in n_1 , the location and amplitude of the obstacle potential are

$$\begin{aligned} x_0(t_{\text{im}} + \Delta t) &= -R_{\text{out}} + v_{\text{ob}} \times (t_{\text{im}} + \Delta t), \\ V_0(t_{\text{im}} + \Delta t) &= V_0(0) - \eta \times (t_{\text{im}} + \Delta t). \end{aligned}$$

Equilibrium TF n_2 within the obstacle potential at this instant of time is

$$n_{2\Gamma}(x, y, t_{\text{im}} + \Delta t) = \frac{\mu_2 - V(x, y, t_{\text{im}} + \Delta t)}{u_{22}}.$$

This, however, is higher than the density distribution at t_{im} , that is $n_{2\Gamma}(x, y, t_{\text{im}} + \Delta t) > n_{2\Gamma}(x, y, t_{\text{im}})$ as the potential V is lower. This is on account of two factors: first, the amplitude of the obstacle potential decreases with time; and second, the harmonic oscillator potential is lower at $x_0(t_{\text{im}} + \Delta t)$. The number of atoms, however, does not change from the value at t_{im} unless there is a strong Josephson current. Density $n_{2\Gamma}$ is thus below the equilibrium value once the obstacle beam is well within n_1 . This creates a stable bubble of n_2 assisted or trapped within the beam and is transported through the n_1 .

Departure of n_2 from the equilibrium is not the only density evolution within the beam. There is a progressive change of $n_{1\Gamma}$ (density of first species within the obstacle beam) as the beam moves deeper into n_1 . At time t_{im} , when the obstacle is completely immersed in n_1 the effective potential, experienced by n_1 , $V(x, y, t_{\text{im}}) + n_{2\Gamma}u_{12}$ is larger than μ_1 . So, n_1 is zero within the beam. However, if the rate of ramping η is such that at a later time $V(x, y, t_{\text{im}} + \Delta t) + n_{2\Gamma}u_{12} < \mu_1$, while the beam is still within n_1 , there is a finite n_1 within the beam. Since $a_{12} > \sqrt{a_{11}a_{22}}$ for the condensate, in TF approximation the bulk values of $n_{1\Gamma}$ and $n_{2\Gamma}$ can not be simultaneously non-zero. At the same time, $n_{2\Gamma}$ is forbidden to migrate to the bulk n_2 due to the n_1 generated potential barrier in the region between interfaces Γ and R_{in} . To accommodate both n_1 and n_2 within the beam, the shape of interface Γ is transformed to increase $n_{2\Gamma}$. So that n_2 is zero in certain regions within the beam where the condition, $V(x, y, t_{\text{im}} + \Delta t) + n_{2\Gamma}u_{12} < \mu_1$, is satisfied. This mechanism is responsible for obstacle assisted transport of n_2 across n_1 .

ENERGETIC STABILITY OF NORMAL VERSUS CORELESS VORTEX DIPOLES

We use TF approximation to compare the energetic stabilities of normal and coreless vortex dipoles.

Normal vortex dipole

Assuming that the vortex affects the density of the condensate only within the core regions, we can adopt the following *ansatz* for binary condensate with a normal

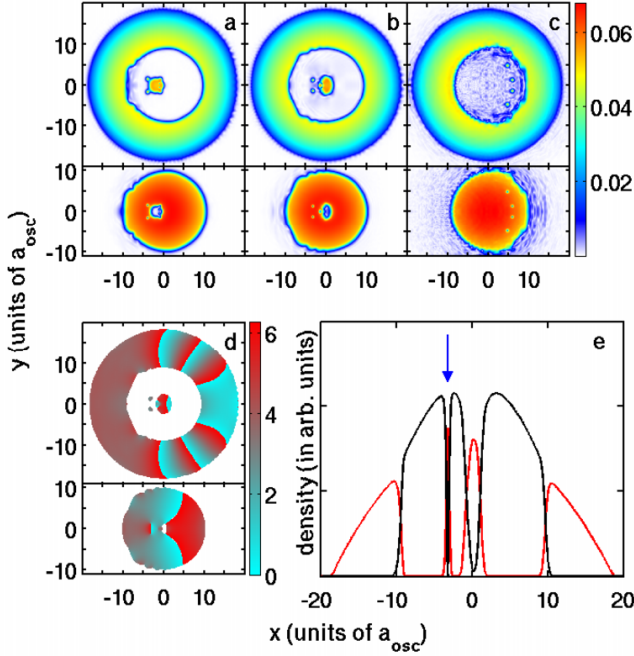


FIG. 2. (Color online) $|\psi_i|$ and phase of binary condensates after the creation of coreless vortex dipole. (a) Coreless vortex dipole is fully formed but yet to dissociate from the obstacle, (b) center of obstacle beam is at origin and coreless vortex dipole is separated, (c) additional coreless vortex dipoles are generated when the obstacle reaches the interface, (d) phase of the binary condensate corresponding to (b), and (e) densities of the condensates parallel to x -axis and passing through the center of the coreless vortex. Blue arrow marks the center of the coreless vortex dipole.

vortex dipole at $(v_1, \pm v_2)$

$$\psi_1(r) = \begin{cases} 0 & x^2 + y^2 > R_{\text{in}}^2 \\ 0 & [(x - v_1)^2 + (y \pm v_2)^2] \leq \xi^2 \\ \sqrt{\frac{\mu_1 - V(x, y)}{u_{11}}} & \begin{cases} x^2 + y^2 \leq R_{\text{in}}^2 & \& \\ [(x - v_1)^2 + (y \pm v_2)^2] > \xi^2 \end{cases} \end{cases} \quad (4)$$

$$\psi_2(r) = \begin{cases} \sqrt{\frac{\mu_2 - V(x, y)}{u_{22}}} & R_{\text{in}}^2 \leq (x^2 + y^2) \leq R_{\text{out}}^2 \\ 0 & (x^2 + y^2) > R_{\text{out}}^2 \\ 0 & (x^2 + y^2) < R_{\text{in}}^2. \end{cases} \quad (5)$$

The vortex dipole contributes mainly through the kinetic energy of ψ_1 , which may be approximated with the value of single species condensate given in Ref.[26]

$$E_{\text{vd}} = \frac{2\mu_1}{u_{11}} \ln \left(\frac{2v_2}{\xi} \right), \quad (6)$$

where $\xi = 1/\sqrt{2\mu_1}$ is the coherence length of inner species. Using these *ansatz* the number of atoms are

$$N_1 = \frac{\pi (1 + 4v_1^2\mu_1 + 4v_2^2\mu_1 - 8\mu_1^2 - 2R_{\text{in}}^4\mu_1^2 + 8R_{\text{in}}^2\mu_1^3)}{8u_{11}\mu_1^2},$$

$$N_2 = \frac{\pi (R_{\text{in}}^2 - 2\mu_2)^2}{4u_{22}}. \quad (7)$$

In a similar way, we can evaluate the energy of the entire condensate.

Coreless vortex dipole

For coreless vortex dipole, we adopt the *ansatz*

$$\psi_1(r) = \begin{cases} 0 & x^2 + y^2 > R_{\text{in}}^2 \\ 0 & [(x - v_1)^2 + (y \pm v_2)^2] \leq \xi^2 \\ \sqrt{\frac{\mu_1 - V(x, y)}{u_{11}}} & \begin{cases} x^2 + y^2 \leq R_{\text{in}}^2 & \& \\ [(x - v_1)^2 + (y \pm v_2)^2] > \xi^2, \end{cases} \end{cases} \quad (8)$$

$$\psi_2(r) = \begin{cases} \sqrt{\frac{\mu_2 - V(x, y)}{u_{22}}} & \begin{cases} R_{\text{in}}^2 \leq (x^2 + y^2) \leq R_{\text{out}}^2 & \parallel \\ [(x - v_1)^2 + (y \pm v_2)^2] \leq \xi^2 \end{cases} \\ 0 & (x^2 + y^2) > R_{\text{out}}^2 \\ 0 & \begin{cases} x^2 + y^2 < R_{\text{in}}^2 & \& \\ [(x - v_1)^2 + (y \pm v_2)^2] > \xi^2. \end{cases} \end{cases} \quad (9)$$

Using these *ansatz* the modified expressions for N_2 is

$$N_2 = \frac{\pi}{8u_{22}\mu_1^2} (2R_{\text{in}}^4\mu_1^2 + 8\mu_1\mu_2 - 8R_{\text{in}}^2\mu_1^2\mu_2 + 8\mu_1^2\mu_2^2 - 1 - 4v_1^2\mu_1 - 4v_2^2\mu_1). \quad (10)$$

As done earlier, we can also calculate the total energy E of the system. The important change in E is the inclusion of interface interaction energy E_{int} . It arises from the interface interactions at the cores of the vortex and antivortex. Based on Ref. [27],

$$E_{\text{int}} = \frac{8}{3} P b \pi \xi \left(\frac{a_{12}}{\sqrt{a_{11}a_{22}}} - 1 \right), \quad (11)$$

where P is the pressure on the circumference of the cores and

$$b = 2 \left[\frac{3(\mu_1 + \mu_2)\sqrt{a_{11}a_{22}}}{4\mu_1\mu_2(a_{12} - \sqrt{a_{11}a_{22}})} \right]^{1/2}. \quad (12)$$

In both the case, i.e. with normal and coreless vortex dipoles, the energy can be minimized with the constraint of the fixed number of atoms and R_{in} as a minimization parameter. For the parameters *set a* without obstacle potential, the coreless vortex dipole has lower energy than the normal vortex dipole and is shown in Fig. 3 for the vortex dipole located at $(0, \pm 1)$.

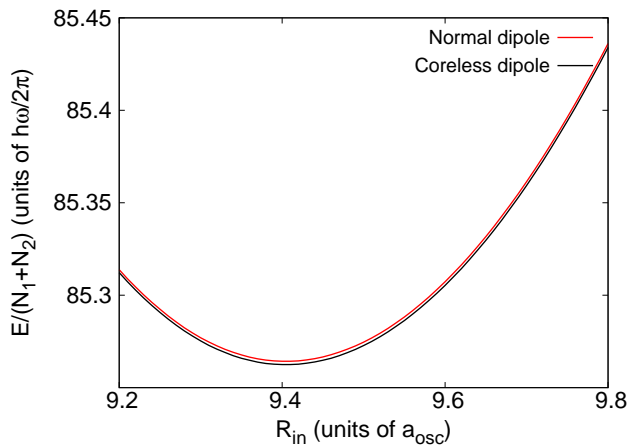


FIG. 3. (Color online) The energy of the binary condensate with $V_0 = 0$ and rest of the parameters same as those in the parameters *set a* as a function of R_{in} . The condensate has a vortex dipole located at $(0, \pm 1)$. Black and blue curves are for coreless and normal vortex dipoles respectively.

For $N_1 = N_2 = 10^6$, $a_{11} = 51a_0$, $a_{22} = 99a_0$ and rest of the parameters same as in parameter *set a*, condensate with the normal vortex dipole has lower energy than the one with coreless vortex dipole (see Fig. 4). These results are in very good agreement with the numerical results.

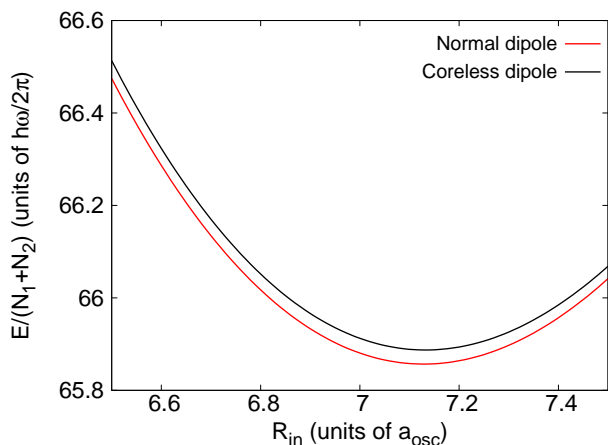


FIG. 4. (Color online) The energy of the binary condensate with $N_1 = N_2 = 10^6$, $a_{11} = 51a_0$, $a_{22} = 99a_0$, $V_0 = 0$, and rest of the parameters same as those in parameters *set a* as a function of R_{in} . The condensate has vortex dipole located at $(0, \pm 1)$. Black and blue curves are for coreless and normal vortex dipoles respectively.

NUMERICAL RESULTS AND CONCLUSIONS

To examine the formation of coreless vortex dipoles in finer detail, we resort to numerical solution of Eq. (2) with a modified version of the split-step Crank-Nicholson

code reported in Ref. [22]. Consider obstacle potential is initially located in the outer component and is moved across the interface, towards the origin. For this case, we consider ^{85}Rb - ^{87}Rb binary condensate with parameters *set a*, however, with maximum value of obstacle laser potential $V_0(0) = 125.0$. The obstacle potential is initially located at $x = -15a_{osc}$. The obstacle moves with the speed of $180\mu\text{m/s}$, progressively decreases in strength with rate constant $\eta = 10.1$ (in scaled units), and vanishes at $x = 8a_{osc}$. The obstacle potential creates a normal vortex dipole as it traverses n_2 . As the obstacle penetrates the interface, it carries the vortex dipole generated in the outer component in its region of influence. Further motion of the obstacle, in n_1 , creates coreless vortices.

The key factor which influences the generation of coreless vortex dipoles is the deformation at the aft region of the obstacle confined n_2 . The deformation accompanied by large mixing is initiated when the interface is about to break up. This is evident even in the stationary state density distribution shown in Fig. 1(b). At break up, the interface repulsion and potential gradient are highest along the x -axis and lead to the formation of a dimple. Curvature is large around the deformed interface, and flow of n_1 past it generates vortex dipoles. However, as the vortex dipoles are generated within the penetration zone, the build up of n_1 around the vortex core drives n_2 from the penetration zone to the core of the vortex. For the parameters considered, first coreless vortex dipole is formed soon after the interface break up and is shown in Fig. 2(a) at $t = 0.21s$. The vortex dipole is almost detached when the obstacle reaches origin, shown in Fig. 2(b). From the phase, Fig. 2(d), it is evident that the phase singularity is associated with n_1 and n_2 is non-zero at the core. This is seen in the plot of densities along a line parallel to x -axis and passing through the vortex core, Fig. 2(e). In the figure, the blue arrow marks the location of the vortex core. Another important density modification is, although the obstacle potential is repulsive, n_2 has a maxima at the center. This is due to the repulsion energy from n_1 . More coreless vortex dipoles are created when the obstacle crosses the center of harmonic potential, 2(c).

The other initial configuration is to place the obstacle potential within n_1 . If V_{obs} is such $\mu_1 < V(\mathbf{r}, t_0) < \mu_2$, then within the obstacle potential n_2 is nonzero. Initial density distribution is like in Figs. 1(c) and 5(a). Due to inertia, n_2 lags behind the beam when the obstacle suddenly starts to move. When the obstacle has shifted from its initial position x_0 to $x_0 + \delta x_0$, the points of intersection of the inner interfaces (assumed circular with radii R_Γ and centered around x_0 and $x_0 + \delta x_0$) are

$$(x_c, y_c) = \left(\frac{1}{2}(2x_0 + \delta x), \pm \frac{1}{2}\sqrt{4R_\Gamma^2 - \delta x^2} \right). \quad (13)$$

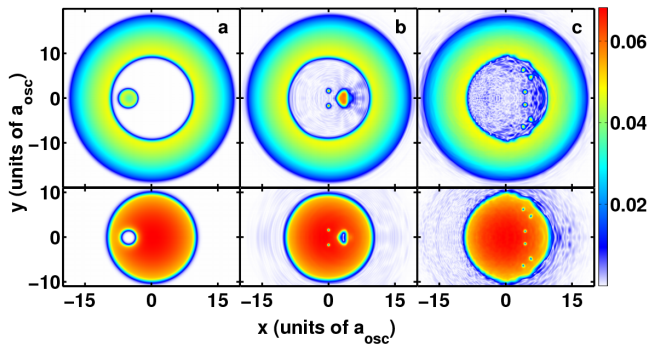


FIG. 5. (Color online) The generation of triply charged vortex dipole in the ^{85}Rb - ^{87}Rb binary condensate with parameters *set a*. The obstacle potential, initially located at $x = -5.0a_{\text{osc}}$, is moved with a velocity of $220\mu\text{m/s}$ up to $x = 5a_{\text{osc}}$. First, second, and third columns are the solutions at $t = 0\text{s}$, $t = 0.14\text{s}$ and $t = 0.32\text{s}$, respectively.

Due to inertia n_2 still occupies the region $\delta\Gamma$ defined as

$$(x - x_0)^2 + y^2 < R_\Gamma^2 < (x - x_0 - \delta x)^2 + y^2$$

The potential experienced by n_2 along the left interface of $\delta\Gamma$ decreases as one moves from x -axis. This leads to redistribution of n_2 in $\delta\Gamma$ region and creation of a pressure difference $\delta P = (n_1^2 u_{11} - n_2^2 u_{22})/2 \geq 0$ at the left bounding arc of $\delta\Gamma$. Along this arc, δP decreases from $(x_0 - R_\Gamma, 0)$ to (x_c, y_c) and tends to flatten it. Another equally important dynamical process is the redistribution of n_1 as $V_{\text{eff}} = V(x, y) + n_2(x, y)u_{12}$ increases along the left interface from x -axis to (x_c, y_c) . Due to this, n_1 start to penetrate the interface from the point where $V_{\text{eff}} \leq \mu_1$. Thus the repulsive interaction at the interface and gradient of harmonic potential, combine to form a dimple. The dimple formation initiates the formation of (coreless) ghost vortices in the obstacle region [28], which detach to form coreless vortex dipoles as is shown in Figs. 5(b)-(c).

We have studied the motion of the Gaussian obstacle across a phase-separated binary condensate. With the possibility of tuning one of the scattering lengths using Feshbach resonances, these condensates can be used to experimentally realise the obstacle assisted transport of one species across another as well as coreless vortices. Using both TF approximation and exact numerical solutions of coupled GP equations, we have shown that coreless vortex dipoles can be energetically more preferable than normal vortex dipoles.

We thank S. A. Silotri, B. K. Mani, and S. Chattopadhyay for very useful discussions. The numerical computations reported in the paper were done on the 3 TFLOPs cluster at PRL. The work of PM forms a part of Department of Science and Technology (DST), Government of

India sponsored research project.

-
- [1] T. W. Neely, E. C. Samson, A. S. Bradley, M. J. Davis, and B. P. Anderson, *Phys. Rev. Lett.* **104**, 160401 (2010).
 - [2] D. V. Freilich, D. M. Bianchi, A. M. Kaufman, T. K. Langin, and D. S. Hall, *Science* **329**, 1182 (2010).
 - [3] B. P. Anderson, P. C. Haljan, C. A. Regal, D. L. Feder, L. A. Collins, C. W. Clark, and E. A. Cornell, *Phys. Rev. Lett.* **86**, 2926 (2001).
 - [4] J. A. Seman, *et al.*, arXiv:1007.4953v4.
 - [5] A. E. Leanhardt, Y. Shin, D. Kielpinski, D. E. Pritchard, and W. Ketterle, *Phys. Rev. Lett.* **90**, 140403 (2003).
 - [6] L. S. Leslie, A. Hansen, K. C. Wright, B. M. Deutsch, and N. P. Bigelow, *Phys. Rev. Lett.* **103**, 250401 (2009)
 - [7] H. Susanto, P. G. Kevrekidis, R. Carretero-Gonzalez, B. A. Malomed, D. J. Frantzeskakis, and A. R. Bishop, *Phys. Rev. A* **75**, 055601 (2007).
 - [8] Yu. G. Gladush, A. M. Kamchatnov, Z. Shi, P. G. Kevrekidis, D. J. Frantzeskakis, and B. A. Malomed, *Phys. Rev. A* **79**, 033623 (2009).
 - [9] A. S. Rodrigues, *et al.*, *Phys. Rev. A* **79**, 043603 (2009).
 - [10] K. Sasaki, N. Suzuki, and H. Saito, *Phys. Rev. A* **83**, 033602 (2011).
 - [11] K. Kasamatsu, and M. Tsubota, *Phys. Rev. Lett.* **93**, 100402 (2004).
 - [12] S. Ronen, J. L. Bohn, L. E. Halmo, and M. Edwards, *Phys. Rev. A* **78**, 053613 (2008).
 - [13] H. Takeuchi, N. Suzuki, K. Kasamatsu, H. Saito, and M. Tsubota, *Phys. Rev. B* **81**, 094517 (2010).
 - [14] S. Gautam, and D. Angom, *Phys. Rev. A* **81**, 053616 (2010).
 - [15] K. Sasaki, N. Suzuki, D. Akamatsu, and H. Saito, *Phys. Rev. A* **80**, 063611 (2009).
 - [16] H. Takeuchi, S. Ishino, and M. Tsubota, *Phys. Rev. Lett.* **105**, 205301 (2010).
 - [17] N. Suzuki, H. Takeuchi, K. Kasamatsu, M. Tsubota, and H. Saito, *Phys. Rev. A* **82**, 063604 (2010).
 - [18] A. Bezett, V. Bychkov, E. Lundh, D. Kobaykov, and M. Marklund, *Phys. Rev. A* **82**, 043608 (2010).
 - [19] C. Hamner, J. J. Chang, P. Engels, and M. A. Hoefer, *Phys. Rev. Lett.* **106**, 065302 (2011).
 - [20] S. B. Papp, J. M. Pino, and C. E. Wieman, *Phys. Rev. Lett.* **101**, 040402 (2008).
 - [21] S. Tojo, Y. Taguchi, Y. Masuyama, T. Hayashi, H. Saito, and T. Hirano, *Phys. Rev. A* **82**, 033609 (2010).
 - [22] P. Muruganandam, and S. K. Adhikari, *Comp. Phys. Comm.* **180**, 1888 (2009).
 - [23] S. L. Cornish, N. R. Claussen, J. L. Roberts, E. A. Cornell, and C. E. Wieman, *Phys. Rev. Lett.* **85**, 1795 (2000).
 - [24] A. A. Svidzinsky and A. L. Fetter, *Phys. Rev. Lett.* **84**, 5919 (2000).
 - [25] B. Jackson, J. .F. McCann, and C. .S. Adams *Phys. Rev. A* **61**, 013604 (1999).
 - [26] Q. Zhou and H. Zhai, *Phys. Rev. A* **70**, 043619 (2004).
 - [27] E. Timmermans, *Phys. Rev. Lett.* **81**, 5718 (1998).
 - [28] K. Fujimoto and M. Tsubota, *Phys. Rev. A* **83**, 053609 (2011).